

## Accurate Iris Localization Using Contour Segments

Haiqing Li, Zhenan Sun and Tieniu Tan

National Laboratory of Pattern Recognition, Institute of Automation  
Chinese Academy of Sciences, Beijing, P.R. China, 100190  
{hqli, znsun, tnt}@nlpr.ia.ac.cn

### Abstract

We consider the problem of locating pupillary and limbic boundaries in iris images captured in non-cooperative environment. This work presents an efficient segment search algorithm, which takes advantage of shape information and learned iris boundary detectors, to enable exclusion of most noisy edges and extraction of genuine pupillary contour segments. Pupillary boundaries can then be accurately fitted as ellipses using the extracted segments. To locate limbic boundaries more stably, the shapes of pupillary boundaries constrain limbic boundary localization by adding inferred points during ellipse fitting. Extensive experiments on the challenging CASIA-Iris-Thousand iris image database demonstrate the effectiveness and efficiency of the proposed method.

### 1. Introduction

Iris localization aims to locate pupillary and limbic boundaries from the background of an iris image, providing important position and region information for further segmentation and iris texture analysis. Because of its crucial role in iris recognition, much attention has been paid during the last two decades [2]. As the development of iris recognition from constrained to non-cooperative environment, iris localization becomes more challenging due to serious noises caused by non-iris regions, such as eyelashes, eyeglass frames and specular reflections.

Great efforts have been made to reduce the impacts of noises to locate iris boundaries accurately and robustly [4, 7, 8]. In our recent work [8], we formulated iris boundary detection in a discriminative framework to distinguish between genuine iris boundary points and spurious ones. Even though the experiments achieved attractive segmentation results in most iris images, the performance will be degraded in non-circular boundary cases because of circle models we used. Moreover, it is inevitable that the learned boundary detectors (LBD for

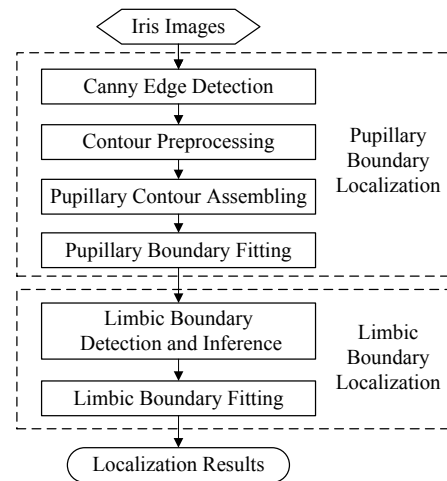


Figure 1: The flowchart of the proposed iris localization method.

short) output false detections. Therefore, more flexible boundary models and further noise removal are needed in the LBD based iris localization method.

Iris boundaries can be modeled as ellipses in most cases [3, 4, 10]. However, such shape information is rarely exploited since every candidate point is treated separately during noise removal [4, 7, 8]. The contours of an object, composed by edge points, contain richer shape information than isolated points. Object detection using contours has been developed in recent years [5, 9]. These methods assemble contour segments into the object outlines under shape constraints and have achieved encouraging performance.

In this paper, we introduce a new iris localization method using contour segments which were ignored in our previous work [8]. The flowchart of the proposed method is shown in Figure 1. We start by preprocessing the Canny edges of an input iris image to get candidate contour segments. Then, an efficient segment search algorithm, which utilizes both shape information and LBD, is designed for genuine pupillary contour

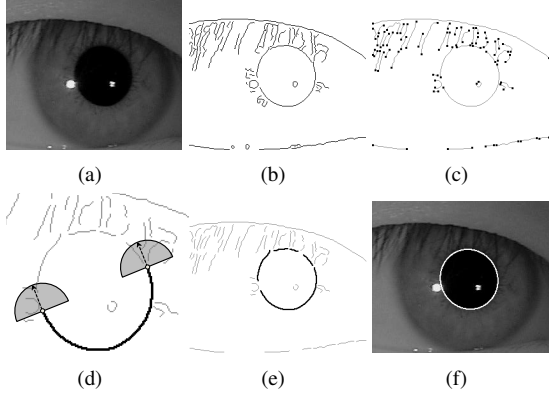


Figure 2: Pupillary boundary localization. (a) Original iris image; (b) Canny edge image; (c) Contour segments, dark points are endpoints; (d) The dark segment is the beginning segment; the semi-circles centered at endpoints illustrate the neighborhood search for adjacent segments; (e) Dark segments are pupillary contour segments after assembling; (f) Pupillary boundary is fitted as an ellipse.

segments assembling. The assembled pupillary contour segments exclude most noises and can be accurately fitted as an ellipse in consequence. After that, limbic boundary points are detected by LBD. For more stable localization results, some unseen limbic boundary points are inferred in eyelid occluded regions. The detected and inferred points are fitted together as an ellipse.

## 2. Technical details

### 2.1. Pupillary and limbic boundary detectors

Learned iris boundary detectors presented in [8] are effective for genuine boundary point detection. We extract the same features as described in [8] to characterize edge points, but employ boosting chain algorithm [11] to train four cascaded AdaBoost boundary detectors, i.e. left/right pupillary and left/right limbic boundary detectors. The cascade structure enables early rejection of spurious points, which accelerates the detection.

### 2.2. Pupillary boundary localization

Shape information of iris boundaries is ignored when the learned boundary detectors classify each edge point separately. In this section, we utilize contour segments to exploit shape information for further noise removal.

We first obtain the candidate pupillary contour segments of an iris image by removing contour junctions and short segments from Canny edges (Figure 2b and 2c). Then, genuine pupillary contour segments are selected from the candidates by pupillary contour assembling algorithm (Algorithm 1).

---

#### Algorithm 1 Pupillary contour assembling and fitting

---

##### Input:

- An iris image and its contour segments  $X = \{S_n\}, n = 1, \dots, N$ , where  $L_n \geq L_{n+1}$ ,  $L_n$  is the length of segments  $S_n$ ;
- Learned left and right pupillary boundary detectors;

##### Initialize:

- Thresholds  $T_p, T_{kl}, T_{ku}$ ;
- Pupillary contour segments  $Y = \emptyset$ ;

##### Find out the beginning segment:

- 1: **for**  $n = 1, \dots, N$  **do**
- 2: Calculate the percentage  $p_n$  of genuine pupillary boundary points validated by LBD in  $S_n$ ;
- 3: Calculate the average curvature  $\kappa_n$  of  $S_n$ ;
- 4: **if**  $p_n > T_p$  **and**  $\kappa_n > T_{kl}$  **and**  $\kappa_n < T_{ku}$  **then**
- 5:  $Y = Y \cup S_n$ ;  $X = X \setminus S_n$ ;
- 6: Contour endpoints  $\{e_{c1}, e_{c2}\} \leftarrow$  The beginning segment endpoints  $\{e_{s1}^n, e_{s2}^n\}$ ;
- 7: Flag  $f_{endp} = 1$ ; **Break**;
- 8: **end if**
- 9: **end for**
- 10: **if**  $Y == \emptyset$  **then**
- 11: No pupillary boundary is found; Goto: **Output**;
- 12: **end if**

##### Assemble pupillary contour segments:

- 13: **while** 1 **do**
- 14: Fit segments in  $Y$  as an ellipse  $B_p$
- 15: **If**  $f_{endp} == 1$ , find adjacent segments near  $e_{c1}$ ; **if**  $f_{endp} == 2$ , find adjacent segments near  $e_{c2}$ . Adjacent segments  $A = \{S_{adjm}\}, m = 1, \dots, M$ , where  $S_{adjm} \in X$ ;
- 16: **if**  $A == \emptyset$  **then**
- 17: **if**  $f_{endp} == 1$  **then**  $f_{endp} = 2$ ;
- 18: **else Break**; **end if**
- 19: **else**
- 20: Update contour segments  $X = X \setminus A$ ;
- 21: Calculate  $c^m$  for each  $S_{adjm}$  (Equation 4);
- 22: Extend pupillary contour segments  $Y = Y \cup S_{best}$ , where  $S_{best}$  is with minimum cost in  $A$ ;
- 23: Update contour endpoints  $\{e_{c1}, e_{c2}\}$ ;
- 24: **end if**
- 25: **end while**

##### Output:

- Pupillary contour segments  $Y$  and ellipse  $B_p$ .
- 

Pupillary contour assembling begins at the most credible pupillary segment (Figure 2d). The beginning segment is fitted as an ellipse  $B_p$  [6] to introduce shape constraints into the following steps. Then the segment with any one of its endpoints in the current contour endpoint's semi-circle neighborhood (Figure 2d) is selected as an adjacent segment and will be evaluated by three cost functions, i.e. LBD cost, angle cost and distance

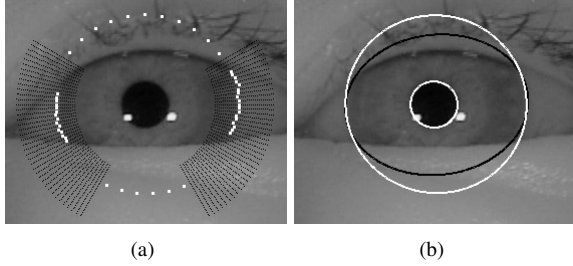


Figure 3: Limbic boundary localization. (a) Limbic boundary points (white points) are detected in the rays (dark lines); unseen limbic boundary points are inferred (white points on upper and lower eyelids); (b) Ellipse fitting without (the dark ellipse) or with (the white ellipse) inferred points.

cost. The LBD cost is:

$$c_{LBD} = g\left(\frac{-2n_p}{a_p + b_p}\right), \quad (1)$$

where  $g(x) = 1/(1 + e^{-x})$  is the logistic function to normalize the cost into  $(0, 1)$ ,  $n_p$  is the number of genuine pupillary boundary points validated by LBD,  $a_p$  and  $b_p$  are semi-major axis and semi-minor axis of  $B_p$  respectively.

The adjacent segment  $s$  is composed by  $L$  points  $(s_1, \dots, s_L)$ , where  $s_1$  and  $s_L$  are the endpoints. Assuming the line determined by  $s_l$  and the center of  $B_p$  intersects  $B_p$  at point  $b_l$ , then the angle cost is calculated as:

$$c_\theta = g\left(\cos^{-1}\left(\frac{\vec{v}_s \cdot \vec{v}_b}{|\vec{v}_s| |\vec{v}_b|}\right)\right), \quad (2)$$

where  $\vec{v}_s$  is the vector from  $s_1$  to  $s_L$ ,  $\vec{v}_b$  is the vector from  $b_1$  to  $b_L$ . The distance cost function is:

$$c_d = g(\mu_d) + g(\sigma_d), \quad (3)$$

where  $\mu_d$  and  $\sigma_d$  are the mean and standard deviation of the distance between  $s_l$  and  $b_l$ , respectively. The total cost is defined as:

$$c = w_{LBD}c_{LBD} + w_\theta c_\theta + w_d c_d, \quad (4)$$

where  $w_{LBD}$ ,  $w_\theta$  and  $w_d$  are weights. Pupillary contour segments are extended by the candidate that has minimum  $c$ .

After several iterations, the genuine pupillary contour segments which exclude most noises are assembled together (Figure 2e). Finally, the pupillary boundary is accurately fitted as an ellipse using the assembled segments (Figure 2f).

### 2.3. Limbic boundary localization

As iris boundary detection in [10], we detect limbic boundary points in rays. Only one point is selected from

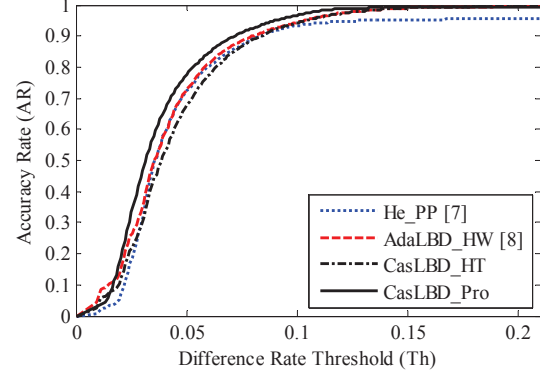


Figure 4: Accuracy rate vs. difference rate threshold on CASIA-Iris-Thousand database.

each ray by learned limbic boundary detectors (Figure 3a). In some cases, only a small number of points can be detected due to occlusions, which may lead to unstable fitting results (e.g., the dark ellipse in Figure 3b).

Since the pupillary boundary has been localized accurately, it will obtain more stable results if assuming that the shape of limbic boundary is similar with the pupillary boundary. Such constraint is added by inferring limbic boundary points in occluded regions. Assuming the unseen points are generated by a latent ellipse which is concentric to the pupillary ellipse, then the parameters of the latent ellipse can be simply deduced by the detected limbic boundary points and the pupillary ellipse. The inferred points are fitted together with the detected points. Therefore, the more inferred points we add, the stronger shape constraint to limbic ellipse fitting. In our experiments, the number of inferred points is less than half of detected points to keep the dominant constraint given by the detected points.

### 3. Experimental results

Experiments are carried out on CASIA-Iris-Thousand database [1]. The database includes 20,000 iris images from 2,000 eyes of 1,000 persons. All images in the database are used for iris localization test. We collect training samples in 200 images which are randomly selected from the first 100 eyes in the database. The number of positive and negative samples for each cascaded AdaBoost detector training are about 10,000 and 100,000 respectively. The patch size is set to  $17 \times 17$  as in [8].

We compare the new method with two state-of-the-art methods proposed in [7] and [8].

To state conveniently, we will use some abbreviations of different localization methods in the rest of the section. Each abbreviation is described as follows:

*He\_PP*: Pupillary and limbic boundaries are localized by the Pulling and Pushing method (PP) [7].

*AdaLBD\_HW*: AdaBoost LBD. Pupillary and limbic circles are determined by weighted Hough transforms [8].

*CasLBD\_HT*: Cascaded AdaBoost LBD. Pupillary and limbic circles are determined by Hough transforms without weighting because the cascaded detectors output only  $\pm 1$ .

*CasLBD\_Pro*: The proposed method described in the previous Section.

The accuracy rate  $AR$  of iris localization is defined in [8]. The average of the semi-major axis and semi-minor axis of an ellipse is used for comparing with the radius of the corresponding circle. The accuracy rate curves varying with the threshold  $Th$  are shown in Figure 4. *CasLBD\_Pro* achieves more accurate localization results than others. Even though *CasLBD\_HT* uses more training samples than *AdaLBD\_HW*, its accuracy is slightly lower than *AdaLBD\_HW*'s, which demonstrates the difficulty to construct both fast and accurate detectors.

Figure 5 shows some examples of localization results. Due to non-circular iris boundaries or serious noises caused by eyeglass frames and reflections, there are some errors in the results of *He\_PP* and *AdaLBD\_HW*. *CasLBD\_Pro* performs better in these images. In rare cases, only a small fraction of pupillary contour segments can be extracted by *CasLBD\_Pro* and cause more unstable localization results than other methods.

We implement *AdaLBD\_HW*, *CasLBD\_HT* and *CasLBD\_Pro* by MATLAB in a PC with 2.4 GHz CPUs. The average time costs per iris localization are about 3.2s, 2.1s and 2.2s respectively, which are slower than *He\_PP* [7]. Benefitting from cascaded detectors, *CasLBD\_HT* is more than one second faster than *AdaLBD\_HW*. The speed of *CasLBD\_Pro* is comparable with *CasLBD\_HT*'s even though iris boundaries are modeled as ellipses rather than circles.

## 4. Conclusions

We have introduced a novel iris localization method using contour segments. Two contributions ensure the superiority of the proposed method. The first one comes from the efficient segment search algorithm which utilizes shape information and LBD to seek out genuine pupillary contour segments. The second one is the shape constraints to limbic boundary localization introduced by inferred points. Extensive experiments on the challenging CASIA-Iris-Thousand iris image database have shown the proposed method achieves state-of-the-art iris localization accuracy.

**Acknowledgements:** This work is funded by the National Basic Research Program of China (Grant No. 2012CB316300),

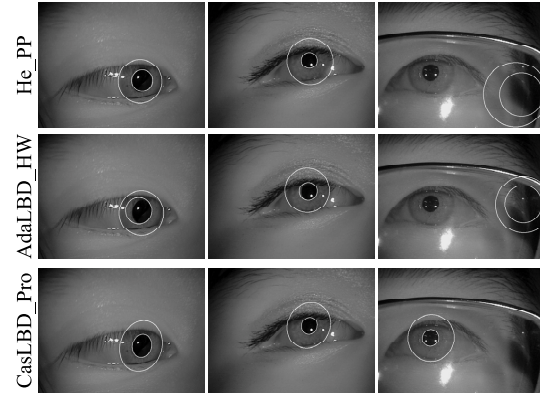


Figure 5: Examples of localization results. From Top to Bottom: Segmentation results by *He\_PP* [7], *AdaLBD\_HW* [8] and *CasLBD\_Pro*.

National Natural Science Foundation of China (Grant No. 60736018, 61075024), International S&T Cooperation Program of China (Grant No.2010DFB14110), National Key Technology R&D Program (Grant No.2012BAK02B01), and the Strategic Priority Research Program of the Chinese Academy of Sciences (Grant No. XDA06030300).

## References

- [1] CASIA Iris Image Database. <http://biometrics.idealtest.org/>.
- [2] K. W. Bowyer, K. Hollingsworth, and P. J. Flynn. Image understanding for iris biometrics: A survey. *Comput. Vis. Image Underst.*, 110(2):281–307, May 2008.
- [3] J. Daugman. New methods in iris recognition. *IEEE Trans. on SMC, Part B*, 37(5):1167–1175, Oct. 2007.
- [4] Y. Du, E. Arslanturk, Z. Zhou, and C. Belcher. Video-based noncooperative iris image segmentation. *IEEE Trans. on SMC, Part B*, 41(1):64–74, Feb. 2011.
- [5] V. Ferrari, T. Tuytelaars, and L. Van Gool. Object detection by contour segment networks. In *Proc. of ECCV*, pages 14–28, 2006.
- [6] A. Fitzgibbon, M. Pilu, and R. Fisher. Direct least square fitting of ellipses. *IEEE Trans. on PAMI*, 21(5):476–480, May 1999.
- [7] Z. He, T. Tan, Z. Sun, and X. Qiu. Toward accurate and fast iris segmentation for iris biometrics. *IEEE Trans. on PAMI*, 31(9):1670–1684, Sept. 2009.
- [8] H. Li, Z. Sun, and T. Tan. Robust iris segmentation based on learned boundary detectors. In *Proc. of ICB*, 2012.
- [9] S. Ravishankar, A. Jain, and A. Mittal. Multi-stage contour based detection of deformable objects. In *Proc. of ECCV*, pages 483–496, 2008.
- [10] W. Ryan, D. Woodard, A. Duchowski, and S. Birchfield. Adapting starburst for elliptical iris segmentation. In *Proc. of BTAS*, Oct. 2008.
- [11] R. Xiao, L. Zhu, and H.-J. Zhang. Boosting chain learning for object detection. In *Proc. of ICCV*, pages 709–715, Oct. 2003.